Journal of Quantitative Spectroscopy & Radiative Transfer 272 (2021) 107774

Contents lists available at ScienceDirect

Journal of Quantitative Spectroscopy & Radiative Transfer

journal homepage: www.elsevier.com/locate/jqsrt

Multilayer selective passive daytime radiative cooler optimization utilizing memetic algorithm

Zafrin Ferdous Mira, Se-Yeon Heo, Do Hyeon Kim, Gil Ju Lee, Young Min Song*

School of Electrical Engineering and Computer Science, Gwangju Institute of Science and Technology, South Korea

ARTICLE INFO

Article history:
Received 24 August 2020
Revised 25 May 2021
Accepted 25 May 2021
Available online 31 May 2021

Keywords:
Transparent atmospheric window
Memetic algorithm
Daytime radiative cooling
Multilayer selective emitter
cooling power
Cooling Temperature

ABSTRACT

Passive Daytime Radiative Cooling (PDRC) process radiates excess heat by dumping heat into space through Transparent Atmospheric Windows (TAWs). Many structures are proposed for the PDRC but their main constraint is achieving near unity selective emission over 8–13 μm (first TAW, *i.e.*, TAW 1) and 16–26 μm (second TAW, *i.e.*, TAW 2) wavelength regions. In this paper, we have presented two Passive Daytime Radiative Coolers (PDRCs) referred as Design 1 and Design 2 which have respectively maximum 99% and 98% emissivity in TAW 1. While Design 1 is simulated considering only TAW 1, Design 2 is found acknowledging both TAW 1 and TAW 2. Both the models consist of three dielectric layers (*i.e.*, SiN, SiC and SiO_2) and a metal (*i.e.*, Ag) back reflector. A genetic algorithm named" Memetic Algorithm" (MA) is utilized to identify the dielectric materials and determine their optimum thickness. The dielectric materials are selected by MA in such a way that their absorption peaks in the TAW 1 do not overlap and destructively interfere with each other, which in turn helps to obtain a high selective emission in that particular window with minimum thickness. This technique can be a new paradigm in designing PDRCs via tailoring material configuration. Additionally, the selective emitters are capable of providing a cooling temperature of 49.8 K and 44 K with a cooling power of 100.72 Wm^{-2} and 112.27 Wm^{-2} at equilibrium respectively for Design 1 and 2 when non-radiative heat exchange coefficient h_c is 0 $Wm^{-2}K^{-1}$ and the studied wavelength range is in between 0.3 to 30 μm. The proposed emitters have only 1D planar layers. Therefore, they can be fabricated with promptly accessible materials which make them a better candidate for large scale fabrication.

1. Introduction

Radiative cooling has recently generated notable interests due to its importance in reducing the temperature of a surface by emitting thermal radiation to the outer space. It has several applications in optoelectronics device [1,2], surface cooling of building [3–5], power plant cooling [6] and spacecraft cooling [7,8]. Passive radiative cooling is such a technique where no external dedicated power supply is necessary to achieve cooling. Due to the energy saving [9] and environment-friendly characteristic [10], passive radiative cooling is gaining popularity in reducing greenhouse gasses [10,11], gain and dissipation of heat in a building [3–5], solar cell cooling [1], etc. It makes use of the mechanism of blackbody emission. Our atmosphere has a transparent atmospheric window over 8 μm to 13 μm wavelength where the absorption is much lower than other regions. This atmospheric window along with blackbody emission at ambient temperature (*i.e.*, around 300 K) provides an optimal opportunity to discharge excess heat into space. As stated in Kirchhoff's law, in a specific wavelength for a material in thermodynamic equilibrium, the absorptivity is equal to the emissivity [12]. Thus, a high selective absorption through 8–13 μm wavelength means achieving high emissivity in that window. There is another window between 16– and 26 μm wavelength but it is depended on atmospheric conditions (fog, moisture, location etc.) [13–15]. Though, the first Transparent Atmospheric Window (*i.e.*, 8–13 μm wavelength region, TAW 1) is our main interest, the second Transparent Atmospheric Window (*i.e.*, 16–26 μm wavelength region, TAW 2) is also taken into consideration in modeling the PDRCs.

Radiative cooling mechanism can be dichotomized into- night and day time cooling [16]. Night-time passive radiative cooling applications started long ago [17–19]. However, most of the research works of day-time passive radiative cooling are still confined in laboratory works. Many broadband and selective emitters are proposed based on metamaterials, polymers, thin films, periodic photonic structures, etc. for passive daytime radiative cooling mechanism. Yet, most of the pioneering works are based on multilayer

* Corresponding author.
E-mail address: ymsong@gist.ac.kr (Y.M. Song).

https://doi.org/10.1016/j.jqsrt.2021.107774
0022-4073/

thin films as the emissivity of the devices can be tailored by varying each layer's characteristics of the multilayer [20]. These structures can lower any surface temperature by 5–11 °C [20–22].

Intermittent films of high index (Titanium Oxide) and low index (silicon-dioxide) materials [23,16], multi-nanolayers of photonic crystal layers [24], dielectric layers optimized with algorithm [25] improve the reflectivity and absorptivity respectively in visible and Infrared (IR) region. However, too many layers would generate high manufacturing cost. In addition, metamaterial emitters with doped periodic photonic structures are burdensome to fabricate on a wide scale as doping of materials is not easy to control [26,27]. Polymer and nano porous coatings are easy to apply in any surface like paint but they are less efficient than metamaterials [26,28].

Though some of the above mentioned works can be fabricated and applied evenly on a surface [21,28], still researchers are looking for the simplest radiative cooling models for practical applications. In this paper, we proposed selective emitters (S.E) consist of dielectric layers of SiN, SiC, SiO_2 and Ag. After finalizing the materials and optimizing the layers' thickness utilizing memetic algorithm, we have found strongly near unity selective emissivity in TAW 1. Emissivity outside the TAWs (*i.e.*, both TAW 1 and TAW 2) is very low. The proposed models are very simple with 1D flat layers without any periodic photonic crystal arrangements (*e.g.* model proposed by Yao et al. [24]) which make them more suitable candidate for smooth fabrication. The overall thickness of the whole structure is only 2.4 μm and 2.3 μm respectively for Design 1 and Design 2. Hence, they can be merged with any silicon structure with a negligible increment of total structure thickness.

2. Design methodology

Selective radiative cooler effectively radiates the heat through TAWs while reflecting in other regions (*i.e.*, UV, visible and Far Infrared; FIR). As other absorption or emission is negligible in TAWs, better cooling performance is observed with higher and selective absorption. It is desired that an ideal selective emitter will have high absorption in TAWs and high reflectivity in other regions [29]. The proposed three layers dielectric selective radiative coolers (TLDSRC) consist of SiN, SiC, and SiO_2 with Ag as a substrate material.

The dielectric layers' and their optimum thickness were finalized using memetic algorithm (MA) [30] which is an expansion of genetic algorithm that integrates local search method in order to avoid getting stuck in a local optimum [31]. MA utilizes the following steps shown in Fig. 1(a) in order to achieve optimized structure and its layers' thickness. Before beginning the optimization process, a target reflectivity spectra of the multilayer structure is defined in the program. At first, MA produces a set of population that is, it randomly produces some layered structures with the specified materials. In the next step, it crossovers between the materials by utilizing same working principle as chromosome crossover shares genetic information in cell division. Different randomly chosen layers and their thickness are arbitrarily modified so that mutation effect of evolution process is observed. Judging each solution by their merit function which is a parameter to measure how much the actual result agrees with the target result, a new set of structures are re-selected for the sake of diversifying the populations. After that, the elite structures' (*i.e.*, structures with small merit function) layer thickness is optimized through local optimization which ensures fast convergence of the program. MA repeats the steps from crossovers to local optimization before arriving at a convergence. The whole optimization process via MA is done in python by specifying target ideal reflectivity spectrum, inserting prospective materials' such as MgF_2, CaF_2, SiC, SiN, SiO_2, PDMS (Polydimethylsiloxane), Ag, etc. refractive indices(n), extinction coefficients(k) values, keeping population number 3000, mutation rate 0.05 and changing the value of the number of layers parameter. At the time of selecting ideal profile, for Design 1 it is regarded that the emitter has low reflectivity in the TAW 1 (*i.e.*, 8–13 μm) and very high reflectivity in all other regions. Moreover, for Design 2, the ideal profile has low reflectivity in both TAW 1 (*i.e.*, 8–13 μm) and TAW 2 (*i.e.*, 16–26 μm) while the remaining regions have high reflectivity.

MA facilitates selective emitter designing process as one can easily specify the target atmospheric windows and prospective materials during the optimization process. A final structure with optimized thickness and materials is found after convergence. In Fig. 1(b), refractive indices(n) and absorption coefficients(k) of the selected materials are presented. The silver (Ag) layer is chosen as a reflector which has high reflectivity along the entire spectrum (*i.e.*, 0.3–30 μm). All of the selected dielectric materials have very low extinction coefficient in solar spectral range (*i.e.*, 0.3–2.5 μm). If a material has high extinction in solar spectrum, it will provide very high absorption but our concern is to get high reflectivity (low absorption) in that particular range [32,33]. Moreover, the absorption coefficients of the chosen materials do not destructively interfere between 8 and 13 μm wavelength. Therefore, a high selective emission is observed between those wavelength ranges.

The final models are simulated in RSoft Diffraction mode. Rsoft is used only to observe optical characteristics of the proposed model without changing any material characteristics and is not included in any optimization process. The models are designed in Rsoft using the optimized thickness and materials found from MA. The refractive index (n) and absorption coefficient (k) values of the chosen materials shown in Fig. 1(b) are inserted in the designed structure in Rsoft. Then emissivity of the models with the change of incident angles, thickness, polarization is simulated. The optimization process utilizing MA is accomplished in python but it can also be coded in MATLAB.

Inserting some of the radiative cooling materials and pairing randomly between them for a predefined result, MA provides a strong selective emission while minimizing maximum number of layers. Utilizing the MA, various optimized layers were found but they are hard to fabricate as some layers are too thick. Prolonged fabrication time because of slow deposition rate at high vacuum condition can degrade the device performance while increasing fabrication cost [34]. Some of these structures are showed in Fig. S1 (supplementary material). Fig. S1(a) is possible to fabricate but the emission is not selective in 8–13 μm wavelength. As a result, we finalized three layers' dielectric emitters considering the fabrication constraints. Fig. 1(c) presents emissivity of Design 1 (*i.e.*, designed taking into account only TAW 1) and Design 2 (*i.e.*, designed considering both TAW 1 and TAW 2). The thickness of each dielectric layers for Design 1 is respectively SiN (0.734 μm), SiC (0.718 μm), and SiO_2 (0.757 μm). As well as, Design 2′s each dielectric layer's thickness is respectively SiN (0.730 μm), SiC (0.272 μm), SiO_2 (1.08 μm). For both the designs Ag is 0.2 μm.

3. Results and discussion

To analyze the efficiency of the radiative cooler, temperature of cooler should be lower than ambient air and the cooling power should be maximized [35]. Utilizing the emissivity data, all other characteristics such as cooling power and cooling temperature are calculated in MATLAB. Maximum achievable cooling power is found from the following equations [29,36].

$$Pcool(Tsample) = Prad(Tsample) - Patm(Tamb) - Psun - P(cond + conv)(Tamb, Tsample) \quad (1)$$

Here, P_{cool} (T_{sample}) is the overall attainable cooling power at given temperature T_{sample}, $P_{rad}(T_{sample})$ is the power radiated by the cooler at given temperature T_{sample}. The absorbed atmospheric radiation at ambient temperature T_{amb} is $P_{atm}(T_{amb})$. The absorbed

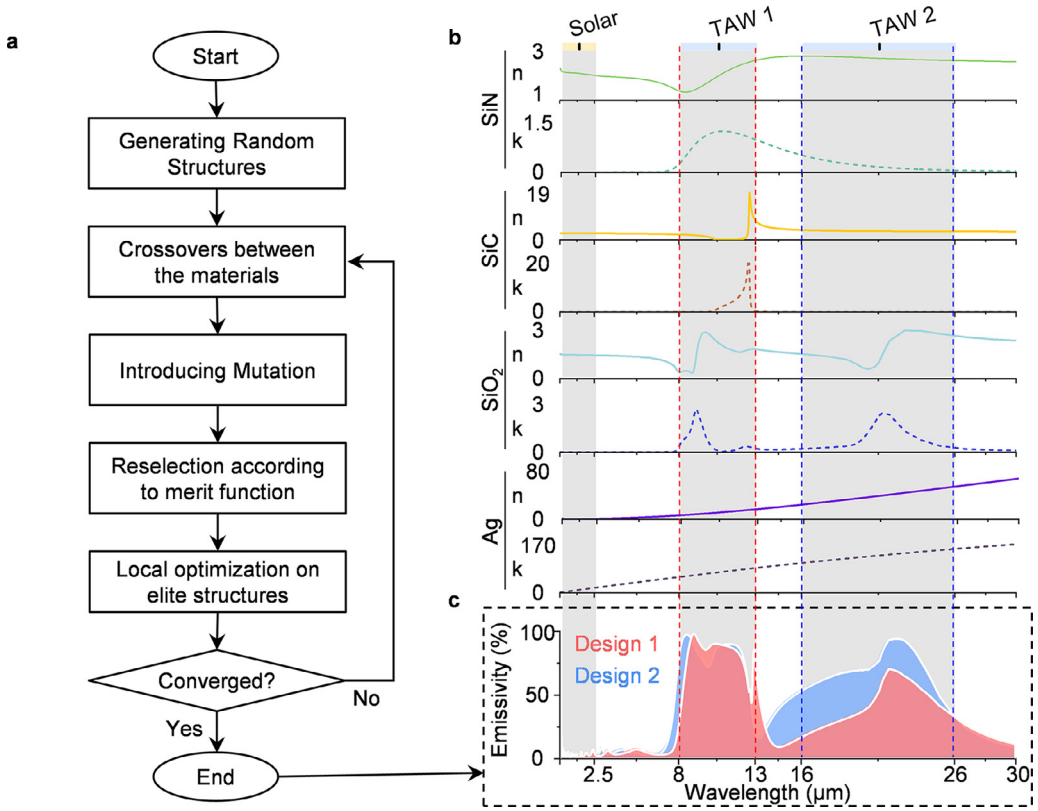

Fig. 1. (a) Flow chart showing individual steps of Memetic Algorithm. (b) Refractive indices (n) and extinction coefficients (k) of SiN, SiC, SiO_2 and Ag utilized to design the selective emitters. (c) Emissivity graph of Design 1 and Design 2 with first Transparent Atmospheric Window (*i.e.*, 8–13 μm referred as TAW 1), second Transparent Atmospheric Window (*i.e.*, 16–26 μm referred as TAW 2) and solar spectrum (*i.e.*, 0.3–2.5 μm).

solar irradiance and nonradioactive heat exchange (*e.g.*, conduction and convection) by cooler is P_{sun} and $P_{(cond+conv)}$ respectively. The radiated power by cooler at given temperature T_{sample} is written as,

$$P_{rad}\left(T_{sample}\right) = A \int \mathrm{d}\Omega cos\theta \int_0^\infty \mathrm{d}\lambda I_{BB}\left(T_{sample}, \lambda\right) \in (\lambda, \theta) \tag{2}$$

Here, $\int d\Omega = 2\pi \int_0^{\pi|2} d\theta \sin\theta$ is the integration in a closed hemisphere. At a particular temperature T_{sample}, the blackbody radiance is found using $I_{BB}(T_{sample}, \lambda) = \frac{2hc^2}{\lambda^5} \frac{1}{e^{\frac{hc}{(\lambda \kappa_B T_{sample})}} - 1}$, where, h is planks constant, c is the velocity of light, k_B is Boltzmann constant, λ is the wavelength. The atmospheric transmittance absorbed by the selective cooler is derived from the equation below,

$$P_{atm}(T_{atm}) = A \int d\Omega cos\theta \int_0^\infty d\lambda I_{BB}(T_{amb}, \lambda)\varepsilon(\lambda, \theta)\varepsilon_{atm}(\lambda, \theta) \tag{3}$$

The angular emissivity at ambient temperature is given by [17],

$$\varepsilon_{atm}(\lambda, \theta) = 1 - t(\lambda)^{1cos\theta} \tag{4}$$

The following equation is required to determine incident solar irradiance absorbed by the selective emitter,

$$P_{sun} = A \int_0^\infty d\lambda \varepsilon(\lambda, \theta_{sun}) I_{AM=1.5}(\lambda) \tag{5}$$

AM 1.5 solar intensity data is employed in this respect.

The equation to calculate absorbed power by the cooler when natural heat exchange process occurs by conduction and convection is,

$$P(cond + conv)(Tsample, Tamb) = h_c(Tamb - Tsample) \tag{6}$$

Here, $h_c = h_{cond} + h_{conv}$ is the accumulated heat exchange coefficient for conduction and convection process. The minimum temperature drops by the radiative cooler is noted comparing the ambient temperature (T_{amb}) and the sample temperature (T_{sample}). At equilibrium condition, the proposed Design 1 can reach a cooling temperature of 51 K with a recognizable daytime cooling power of 91 Wm^{-2} considering the emissivity between 0.3–20 μm wavelength and without taking into account non-radiative heat exchange (*i.e.*, conduction and convection) mechanism. It shows low emissivity in the solar and near-infrared regions (*i.e.*, 0.3–4 μm) which is a desirable characteristic of the selective PDRC. Fig. 2(a) presents emissivity of the Design 1 in solar range (*i.e.*, 0.3–2.5 μm) with normalized AM 1.5 solar spectrum.

The proposed Design 1 exhibits high selective emission in TAW 1 (Fig. 2(b)). All data of Fig. 2 are simulated with Mauna kea sky transmission with water column 1 mm [37]. The first dip which is approximately at 9 μm wavelength is due to the longitudinal vibrational modes of SiO_2 and the second dip is caused by SiC at 13 μm wavelength. This dip can be removed if we exchange SiC with suitable materials. However, SiC is very significant in these particular models to achieve selective emission. Moreover, we noticed that increasing SiO_2 and SiC layers (*i.e.*, four consecutive layers of SiO_2 and SiC with top SiN layer and bottom Ag layer) for Design 1 considering wavelength region 0.3 to 20 μm the emissivity between 8 and 13 μm wavelength increases in a small quantity (Fig. S2 (supplementary materials)). As the increment is not significant (*i.e.*, difference of cooling temperatures and cooling powers are 3 K and 1 Wm^{-2} respectively at h_c=0 $Wm^{-2}K^{-1}$) and considering simplicity in fabrication, we proposed the 3-layer dielectric selective emitters with a back metal reflector.

Comparison between our recommended Design 1 which shows high cooling temperature than Design 2 and published models provide a better insight about the whole situation. The cooling power with respect to the cooling temperature for Mauna kea sky transmission [37] is shown in Fig. 2(c). Design 1 cooler's cooling performance is compared with three well-known published articles.

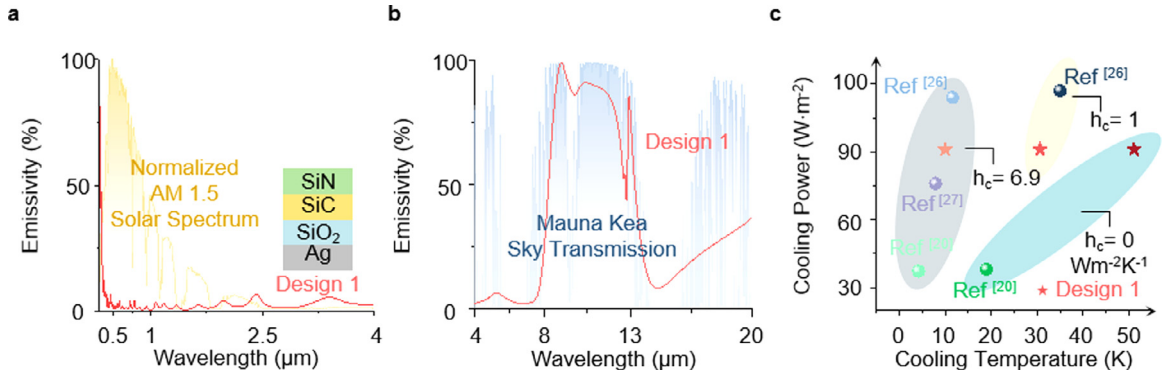

Fig. 2. (a) Normalized spectral intensity (AM 1.5 solar spectrum) with emissivity of the proposed Design 1 at solar and near infrared regions (*i.e.*, 0.3 to 4 μm wavelength). (b) Emissivity graph of Design 1 with Mauna kea sky Transmission for water column of 1 mm. (c) Comparison between cooling power with respect to cooling temperature (T_{amb}-T_{sample}) K of Design 1 and Refs. [20,26,27] for h_c=0, 1, 6.9 $Wm^{-2}K^{-1}$.

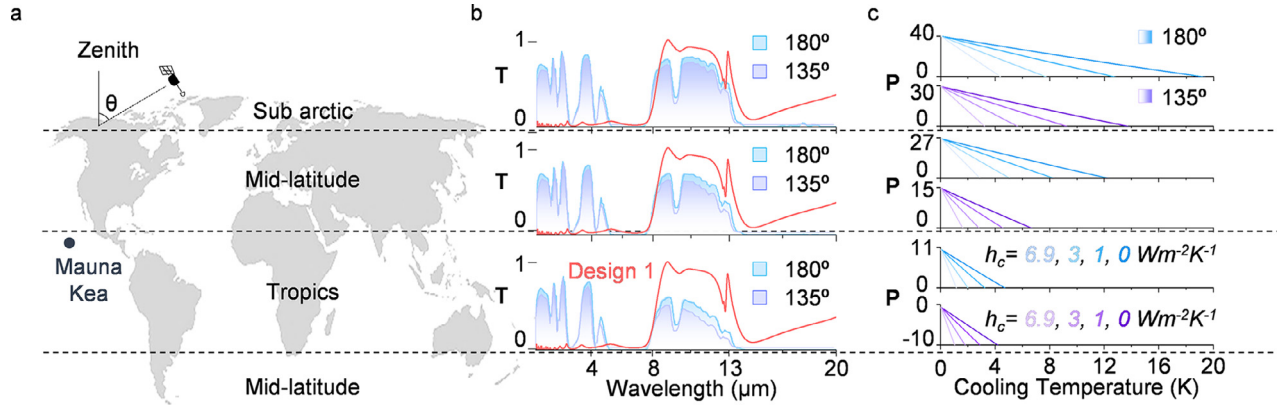

Fig. 3. (a) Global climate map showing sub-arctic, mid-latitude and tropics regions. (b) Performance analysis of Design 1 considering sky transmission of sub-arctic summer, mid-latitude summer and tropics with moisture content of respectively 2589.4 atm-cm, 3635.9 atm-cm, 5119.4 atm-cm and sensor zenith of 180 and 135°. (c) Cooling Power *vs.* Cooling temperature(T_{amb}-T_{sample}) K with the variation of h_c from 0 to 6.9 $Wm^{-2}K^{-1}$ for the data plotted in Fig. 3(b).

Without considering the non-radiative heat exchange coefficient (h_c=0 $Wm^{-2}K^{-1}$), Design 1 provides high cooling temperature of 51 K with a cooling power of 91 Wm^{-2} at equilibrium when the wavelength range is between 0.3 to 20 μm wavelength. Cooling temperature is greater than that of Raman et al. [20], Zou et al. [27], and Hossain et al. [26]. Non-radiative heat exchange coefficient, h_c can be varied to determine how the convective and conductive heat exchange process is affecting the cooling device's performance. Varying h_c up to 6.9 $Wm^{-2}K^{-1}$ is sufficient, if the device is working at ambient temperature in low moisture conditions [29,38]. When h_c is varied, the Design 1 does not provide better performance than that of Hossain et al. [26], but provides relatively better result than that of Raman et al. [20] and Zou et al. [27]. In addition, when h_c is 1 $Wm^{-2}K^{-1}$ and 6.9 $Wm^{-2}K^{-1}$, at equilibrium cooling temperature below the ambient temperature are 30 K and 10 K respectively. We have also simulated the Design 1 emitter's performance with different input parameters adapted from MODTRAN [14,15]. The Fig. 3(a) displays global climate map of different regions such as sub-arctic, mid-latitude, tropics in summer season. Sky transmission of the above-mentioned respective locations are presented side by side in Fig. 3(b). The emissivity of proposed Design 1 is also included in the same figure for reference purpose. In all cases, the highest moisture content and two different sensor zenith angles (angle between zenith and sensing point, Fig. 3(a)) are regarded at the time of retrieving data from MODTRAN so that we can realize how Design 1 will perform during bad weather conditions.

Design 1 cooler's cooling performance at sub-arctic summer, mid-latitude summer and tropics with water column of respectively 2589.4 atm-cm, 3635.9 atm-cm, 5119.4 atm-cm and sensor zenith of 180 and 135° is presented in Fig. 3(c). Cooling temperature varies from 19.2 K to 4 K with a cooling power of 40 Wm^{-2} for subarctic summer considering sensor zenith 180°. The non-radiative heat exchange coefficient, h_c is varied between 0 and 6.9 $Wm^{-2}k^{-1}$. On the other hand, changing the sensor zenith to 135°, the sky transmission changes which also affects the cooling performance and cooling temperature lowers to 13.6 K for h_c=0 $Wm^{-2}k^{-1}$ in subarctic summer condition. Altering sensor zenith angles and non-radiative heat exchange coefficient for mid-latitude summer condition similar behavior like sub-arctic sum-

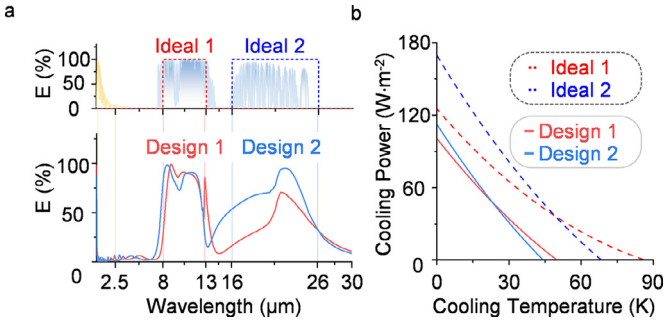

Fig. 4. (a) Emissivity of Ideal 1 considering only TAW 1 *i.e.*, 8–13 μm and Ideal 2 considering both TAW 1 and TAW 2 (*i.e.*, 8–13 μm and 16–26 μm) including emissivity profiles of Design 1 and Design 2 with Mauna kea sky transmission water column 1 mm. (b) Analysis of cooling performance for Design 1, Design 2, Ideal 1 and Ideal 2.

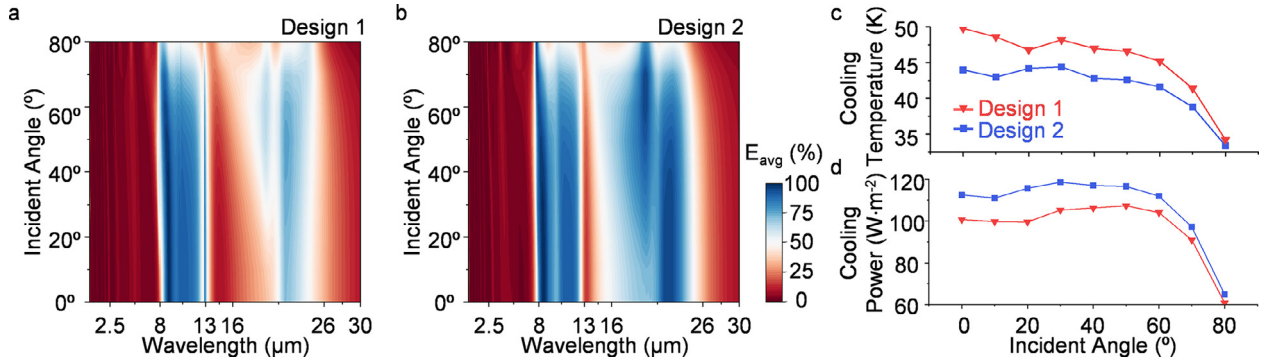

Fig. 5. (a) Contour plot for average emissivity (average of TE and TM polarization) of Design 1 with variation of angle from 0 to 80° between the wavelength of 0.3 to 30 μm. (b) Contour plot for average emissivity of Design 2 with respect to changing angles. (c) Cooling temperature calculation of Design 1 and 2 with the changing of angles. (d) Cooling power *vs.* Incident angle determined for Design 1 and 2.

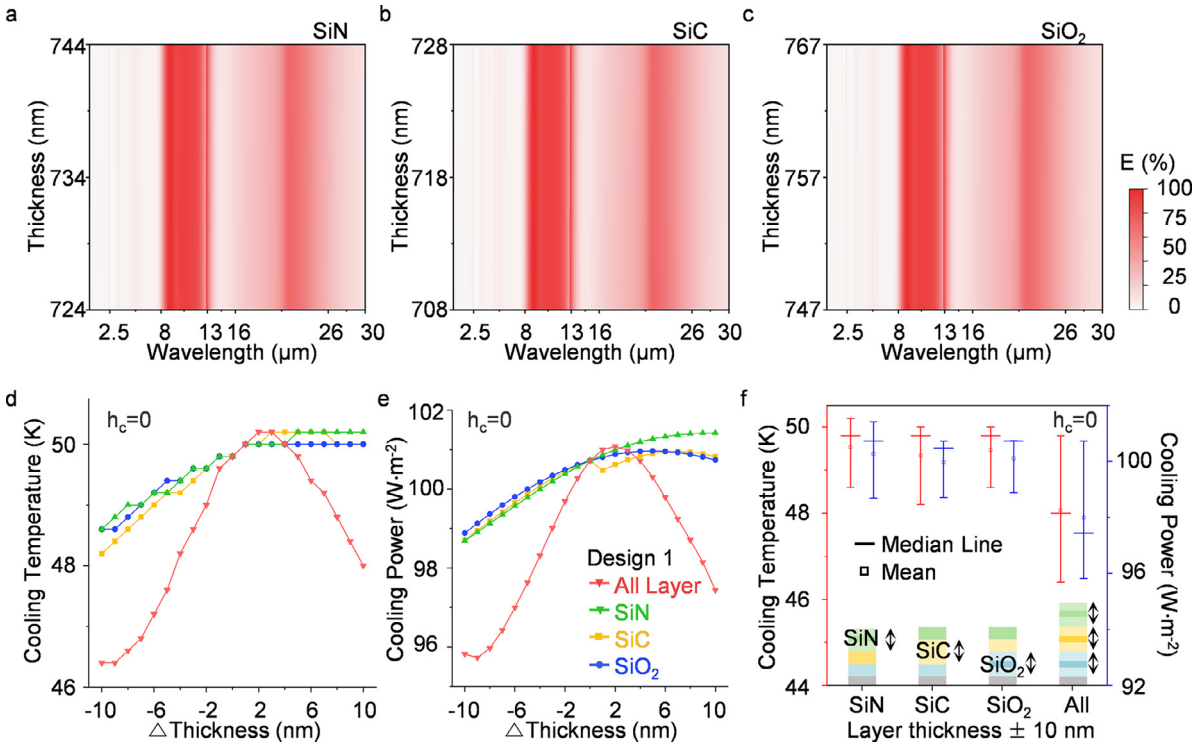

Fig. 6. Contour plots changing the thickness of (a)SiN (b)SiC, (c)SiO_2 between ±10 nm from the original thickness for Design 1 while considering the thickness of other two layers and Ag unchanged (d) Cooling temperature *vs.* thickness variation of only SiN, SiC, SiO_2 and all three dielectric layers for Design 1. (e) Cooling power *vs.* thickness variation of only SiN, SiC, SiO_2 and all three dielectric layers for Design 1. (f) Box plot showing cooling temperature and cooling power *vs.* thickness variation between −10 to +10 nm for Design 1.

mer in terms of cooling performance is observed. Cooling power at equilibrium for mid-latitude summer sky transmission is 26.5 Wm^{-2} taking sensor zenith 180°. Furthermore, the cooler Design 1 shows least desirable cooling performance in tropics due to having exceedingly high moisture content comparing with the other two sky transmissions of sub-arctic and mid latitude summer. Excessive water content in atmosphere greatly affects the cooling efficiency. Thus, Design 1 is unable to provide cooling in tropics when the water column is 5119.4 atm-cm and sensor zenith 135°.

Even though we considered only the TAW 1 (*i.e.*, 8–13 μm) during the modeling process of Design 1, there is a TAW 2 (*i.e.*, 16–26 μm) and it is dependent on atmospheric conditions. When both the windows are considered, it changes the cooling temperature and power of the radiative coolers. Taking into account various combination of first and second atmospheric windows and changing ideal profiles, numerous passive radiative coolers can be designed and applied in respective weather conditions [39,40]. Adapting both TAW 1 and TAW 2 efficient cooling performance can be observed at daytime [39]. As our proposed emitter is designed to serve at daytime, we have mentioned another cooler referred to as Design 2 which is designed utilizing MA and keeping in mind both TAW 1 and TAW 2. The TAW 2 is recognized from 16 to 26 μm according to [13]. It is also implicated during the cooling performance analysis of Design 2. It consists of the same materials and number of layers as Design 1 and the thickness for each layers is mentioned earlier. In Fig. 4(a), the emissivity of Design 1 with ideal emissivity profile inspects only TAW 1 (referred as Ideal 1) and Design 2 considers both TAW 1 and TAW 2 which is referred as Ideal 2. Mauna kea sky transmission with water column 1 mm can be found on the same figure. During the optimization process for Design 1, only TAW 1 is regarded and for this reason it can only provide maximum 70% emissivity in the TAW 2. With the intention

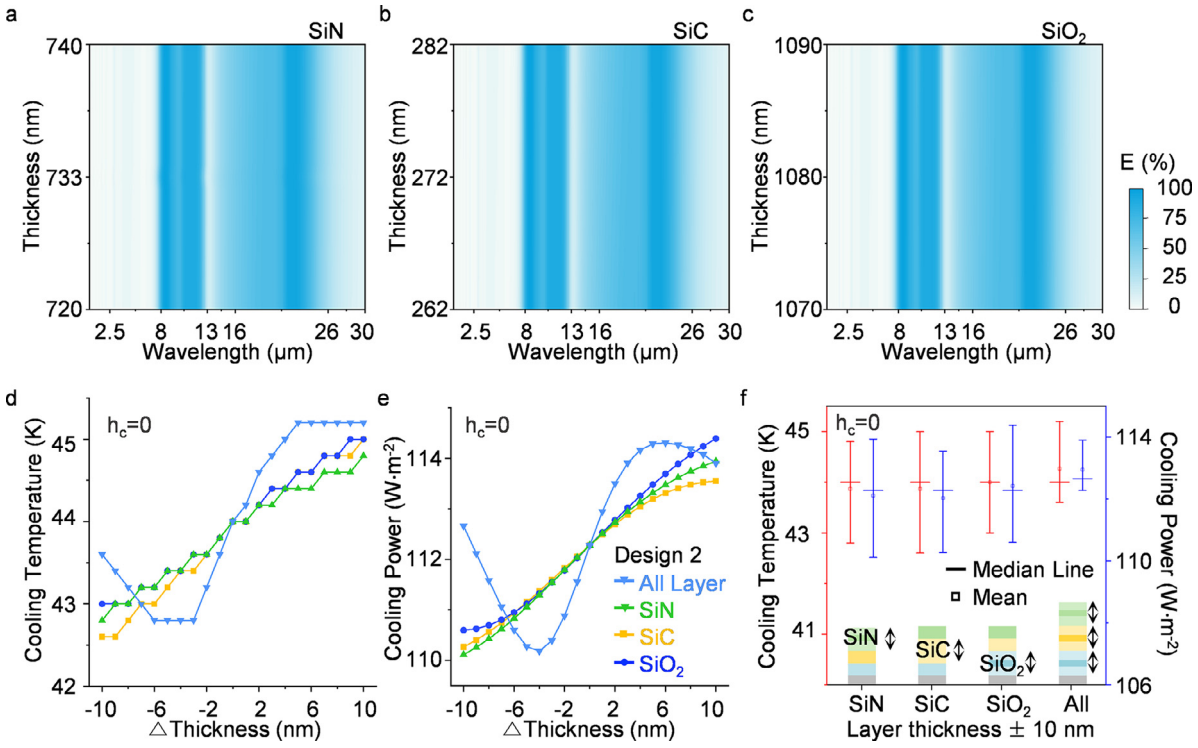

Fig. 7. Contour plots changing the thickness of (a)SiN (b)SiC, (c)SiO_2 between ±10 nm from the original thickness for Design 2 while considering the thickness of other two layers and Ag unchanged (d) Cooling temperature *vs.* thickness variation of only SiN, SiC, SiO_2 and all three dielectric layers for Design 2. (e) Cooling power *vs.* thickness variation of only SiN, SiC, SiO_2 and all three dielectric layers for Design 2. (f) Box plot showing cooling temperature and cooling power *vs.* thickness variation between −10 to +10 nm for Design 2.

of improving emissivity in the TAW 2, the thickness of the three dielectric layers are altered by MA. Design 2 which is designed including both TAW 1 and TAW 2 shows 24% improvement in terms of comparing with maximum emissivity of Design 1 in TAW 2. But the emissivity in the TAW 2 is not selective like TAW 1 and the dip seen in 9 μm is degraded in Design 2.

There is always a trade-off between the cooling power and cooling temperature of PDRCs. A high cooling power does not necessarily associate with a high cooling temperature. In Fig. 4(b) cooling power is estimated for Ideal 1, Ideal 2, Design 1 and Design 2 between the wavelength range of 0.3 to 30 μm and assuming h_c=0. When only TAW 1 (*i.e.*, 8–13 μm) is considered, the Ideal 1 can attain a high cooling temperature of 86.4 K below the ambient temperature. Yet, a high cooling power of 169.7 Wm^{-2} is obtained with Ideal 2. It can lower the surface temperature by 68.4 K. As both the ideal coolers intercept each other at a cooling temperature of 49.2 K and a cooling power of 36.47 Wm^{-2}, so it can be realized with both the ideal coolers. Design 1 is able to reach a cooling temperature of 49.8 K considering wavelength 0.3–30 μm below the ambient temperature and a cooling power of 100.72 Wm^{-2} at equilibrium state. For Design 2 though cooling power increases by 11.87 Wm^{-2}, cooling temperature decreases by 5.8 K contrasting with Design 1. The absolute value of the slope of Design 2 (*i.e.*, 3.13) is steeper than Design 1 (*i.e.*, 2.57), which's why Design 2 is more tilted downwards. Moreover, Design 2 has a higher y-intercept (*i.e.*, 154.13) than Design 1 (*i.e.,* 135.78) which is also the reason for the Design 2 plot's being steeper. These values of slopes and intercepts are calculated considering the whole data set. Due to having steeper slopes, Design 2 loses its cooling temperature more rapidly than Design 1 with the increasing of cooling temperature. Considering individual points of cooling power *vs*. cooling temperature curves, slopes are being calculated for discrete points and plotted against cooling temperature of the coolers which can be noticed in Fig. S3 of supplementary material. Respectively comparing with Ideal 1 and Ideal 2, we can observe that Design 2 has higher slopes than its ideal profile. Hence, with the increasing of temperature slopes are increasing and thereby design 2 achieves high cooling power at lower temperature than Design 1. Therefore, Design 2 can be utilized when a high cooling power is needed.

Angle dependency highly affects the cooling performance of the radiative coolers. How emissivity changes with the variation of incident angles for Design 1 and Design 2 are respectively shown in Fig. 5(a) and Fig. 5(b). The responses are found by averaging Transverse Electric (TE) and Transverse magnetic (TM) waves as both TE and TM waves are found in solar irradiation. Average emissivity reaches 81% for both Design 1 and 2 in the TAW 1 (*i.e.*, between 8 and 13 μm). At higher angles the selectivity degrades in the TAW 1. From Fig. 5(a) and Fig. 5(b), it is noticed that both Design 1 and 2 show high selectivity up to angle 60°. Moreover, in case of Design 1 low variation of emissivity is identified in TAW 2 with the variation of angle. Although high emissivity is observed for design 2 in TAW 2, it is greatly dependent on angles. So, Design 1 and 2 both have great resistance to angle in the TAW 1. We have also examined cooling performance of both the designs with the variation of angle and the results are incorporated in Fig. 5(c) and 5(d). Both the designs' cooling temperature and cooling power is sustained in between 30 and 60°' angle.

Furthermore, we have analyzed thickness variation of Design 1 and 2 in order to comment on how much thickness variation during fabrication will not hinder the cooler's performance. Fig. 6(a), 6(b) and 6(c) show the contour plots for Design 1 from 0.3 to 30 μm wavelength varying the respective layer thickness ±10 nm from their simulated thickness (*i.e.*, SiN=734 nm, SiC=718 nm, SiO_2=757 nm) and keeping all other layer's thickness unchanged. It can be undoubtedly said that the emissivity profile in the TAW

1 encounters negligible changes when the thickness of each respective layers is varied subsequently. Hence, Design 1 has great resistance to thickness variation during fabrication. Additionally, varying the layer thickness cooling power and temperature are inspected and sequentially presented in Fig. 6(d) and 6(e). Varying all layers' thickness from −10 nm to +10 nm, maximum cooling temperature and cooling power changes are respectively 3.4 K and 4.8 Wm^{-2} comparing with simulated Design 1. Variation of cooling power and temperature is not significant taking into account individual layer changes. From Fig. 6(f), it is observed that for all layers' thickness variation from −10 to +10 nm cooling temperature fluctuates from 46.4 K to 49.8 K and cooling power changes from 95.8 Wm^{-2} to 100.72 Wm^{-2}. Thickness variation for Design 2 is also calculated. According to Fig. 7(a), 7(b), 7(c), contour plots of Design 2 show minor changes in its emissivity by the thickness alteration from their optimized thickness (*i.e.*, SiN=730 nm, SiC=272 nm, SiO_2=1080 nm) via MA. Given the thickness variation for all dielectric layers from −10 to 10 nm, maximum changes in cooling temperature and power faced by Design 2 are respectively 1.2 K and 2 Wm^{-2} exhibited in Fig. 7(d), 7(e). Besides, we can easily identify the ranges of cooling power and temperature for thickness alteration from −10 to +10 nm from Fig. 7(f). Cooling power ranges in between 112 and 113 Wm^{-2} considering alteration of all three dielectric layers. So, Design 1 and 2 both show good resistance to the layer thickness variation. In some cases, cooling performance is improved in small quantity after the thickness alteration presented in Figs. 6 and 7. As a result, we can say that MA provides structures close to the best structure after optimization process. As the discrepancy is not significant, it can certainly be utilized in designing feasible PDRCs.

4. Conclusion

In a nut shell, we have suggested three-layer dielectric selective daytime radiative coolers with a metal back reflector. The dielectric materials and their thickness is optimized utilizing memetic algorithm which is an evolutionary genetic algorithm developed on the basis of Darwinism [41]. The Optimized thickness for the dielectric layers of Design 1 is 0.734 μm, 0.718 μm and 0.757 μm respectively for SiN, SiC and SiO_2. Design 2′s optimum thickness of each dielectric layer is respectively SiN (0.730 μm), SiC (0.272 μm), SiO_2 (1.08 μm). Both the designs have a Ag back reflector which is 0.2 μm. Design 1 is optimized in MA only considering TAW 1 (*i.e.*, 8–13 μm). While Design 2 is obtained taking into consideration both the TAW 1 and TAW 2 (*i.e.*, 8–13 μm and 16–26 μm). At equilibrium state, the proposed Design 1 and 2 respectively provide a cooling temperature of 49.8 K and 44 K below the ambient temperature with a cooling power of 100.72 Wm^{-2} and 112.27 Wm^{-2} without considering non-radiative heat exchange (*i.e.*, conduction and convection) and assuming the wavelength range in between 0.3–30 μm wavelength. The finalized Design 1 and Design 2 models respectively display 99% and 98% maximum emissivity with an average high emission of 81% for both the coolers over 8–13 μm wavelength. Furthermore, the materials elected by MA demonstrate very high selective emission in TAW 1 as the absorption peaks of the materials do not overlap in that range. Hence, tailoring absorption peaks can be regarded as a crucial step in designing radiative coolers. Our proposed selective emitters will be easy to fabricate because of their planar 1D layered structures. The devices' performance is simulated in different weather conditions ensuring that they can be a good alternative where daytime cooling is necessary. Additionally, the coolers can be easily integrated with silicon photonics (*e.g.* solar cell) and electronics to remove excess heat but small change is crucial for this purpose.

Declaration of Competing Interest

The authors declare that they have no known competing financial interests or personal relationships that could have appeared to influence the work reported in this paper.

CRediT authorship contribution statement

Zafrin Ferdous Mira: Writing – original draft, Conceptualization, Software, Data curation, Writing – review & editing, Investigation. **Se-Yeon Heo:** Conceptualization, Visualization, Writing – review & editing, Investigation. **Do Hyeon Kim:** Writing – review & editing, Investigation. **Gil Ju Lee:** Writing – review & editing, Investigation. **Young Min Song:** Supervision, Project administration, Writing – review & editing, Investigation.

Acknowledgments

This work was supported by the National Research Foundation of Korea (NRF) funded by the Korean government (MSIP) (Grants NRF2018R1A4A1025623, NRF 2018M3D1A1058997, and NRF2020R1A2C2004983). Also, this work was supported by the Korea Institute of Energy Technology Evaluation and Planning (KETEP) and by the Ministry of Trade, Industry and Energy (MOTIE) of the Republic of Korea (Grant No. 20183010014310). Zafrin Ferdous Mira and Se-Yeon Heo contributed equally to this work.

Supplementary materials

Supplementary material associated with this article can be found, in the online version, at doi:10.1016/j.jqsrt.2021.107774.

References

[1] Zhu L, Raman A, Wang KX, Anoma MA, Fan S. Radiative cooling of solar cells. Optica 2014;1(1):32–8.
[2] Kang MH, Lee GJ, Lee JH, Kim MS, Yan Z, Jeong J-W, et al. Outdoor-useable, wireless/battery-free patch-type tissue oximeter with radiative cooling. Adv Sci 2021;8(10):2004885.
[3] Al-Obaidi KM, Ismail M, Abdul Rahman AM. Passive cooling techniques through reflective and radiative roofs in tropical houses in southeast asia: A literature review. Front Archit Res 2014;3(3):283–97.
[4] Lu X, Xu P, Wang H, Yang T, Hou J. Cooling potential and applications prospects of passive radiative cooling in buildings: the current state-of-the-art. Renew Sust Energ 2016;65:1079–97.
[5] Wang W, Fernandez N, Katipamula S, Alvine K. Performance assessment of a photonic radiative cooling system for office buildings. Renew Energy 2018;118:265–77.
[6] Zeyghami M, Khalili F. Performance improvement of dry cooled advanced concentrating solar power plants using daytime radiative cooling. Energy Convers Manag 2015;106:10–20.
[7] Kim H, Cheung K, Auyeung RCY, Wilson DE, Charipar KM, Piqué A, Charipar NA. Vo2-based switchable radiator for spacecraft thermal control. Sci Rep 2019;9(1):11329.
[8] Sun K, Riedel CA, Wang Y, Urbani A, Simeoni M, Mengali S, Zalkovskij M, Bilenberg B, de Groot CH, Muskens OL. Metasurface optical solar reflectors using azo transparent conducting oxides for radiative cooling of spacecraft. ACS Photonics 2018;5(2):495–501.
[9] Smith G, Gentle A. Radiative cooling: energy savings from the sky. Nat Energy 2017;2(9):17142.
[10] Liu C-H, Ay C, Tsai C-Y, Lee M-T. The application of passive radiative cooling in greenhouses. Sustainability 2019;11(23):6703.
[11] Heo S-Y, Lee GJ, Kim DH, Kim YJ, Ishii S, Kim MS, Seok TJ, Lee BJ, Lee H, Song YM. A janus emitter for passive heat release from enclosures. Sci Adv 2020;6(36).
[12] Tian Y, Ghanekar A, Qian L, Ricci M, Liu X, Xiao G, Gregory O, Zheng Y. Near-infrared optics of nanoparticles embedded silica thin films. Opt Express Feb 2019;27:A148–57.
[13] Kong A, Cai B, Shi P, Yuan X-c. Ultra-broadband all-dielectric metamaterial thermal emitter for passive radiative cooling. Opt Express 2019;27(21):30102–15.
[14] Berk A, Conforti P, Kennett R, Perkins T, Hawes F, van den Bosch J. *MODTRAN6: a major upgrade of the MODTRAN radiative transfer code*, vol. 9088 of *SPIE Defense + Security*. SPIE; 2014.
[15] Berk A, Conforti P, Hawes F. *An accelerated line-by-line option for MODTRAN combining on-the-fly generation of line center absorption within 0.1 cm-1 bins and pre-computed line tails*, vol. 9472 of *SPIE Defense + Security*. SPIE; 2015.

[16] Liu T, Takahara J. Ultrabroadband absorber based on single-sized embedded metal-dielectric-metal structures and application of radiative cooling. Opt Express Jun 2017;25:A612–27.
[17] Granqvist CG, Hjortsberg A. Radiative cooling to low temperatures: General considerations and application to selectively emitting sio films. J Appl Phys 1981;52(6):4205–20.
[18] Dong M, Chen N, Zhao X, Fan S, Chen Z. Nighttime radiative cooling in hot and humid climates. Opt Express 2019;27(22):31587–98.
[19] T.Q. Pean, L. Gennari, B.W. Olesen, and O.B. Kazanci, "Nighttime radiative cooling potential of unglazed and pv/t solar collectors: parametric and experimental analyses," 2015.
[20] Raman AP, Anoma MA, Zhu L, Rephaeli E, Fan S. Passive radiative cooling below ambient air temperature under direct sunlight. Nature 2014;515(7528):540–4.
[21] Kou J-l, Jurado Z, Chen Z, Fan S, Minnich AJ. Daytime radiative cooling using near-black infrared emitters. ACS Photonics 2017;4(3):626–30.
[22] Suichi T, Ishikawa A, Hayashi Y, Tsuruta K. *Structure optimization of metallodielectric multilayer for high-efficiency daytime radiative cooling*, vol. 10369 of *SPIE Optical Engineering + Applications*. SPIE; 2017.
[23] Kecebas MA, Menguc MP, Kosar A, Sendur K. Passive radiative cooling design with broadband optical thin-film filters. J Quant Spectrosc Radiat Transf 2017;198:179–86.
[24] Yao K, Ma H, Huang M, Zhao H, Zhao J, Li Y, Dou S, Zhan Y. Near-perfect selective photonic crystal emitter with nanoscale layers for daytime radiative cooling. ACS Appl Nano Mater 2019;2(9):5512–19.
[25] Chae D, Kim M, Jung P-H, Son S, Seo J, Liu Y, Lee BJ, Lee H. Spectrally selective inorganic-based multilayer emitter for daytime radiative cooling. ACS Appl Mater Interfaces 2020;12(7):8073–81.
[26] Hossain MM, Jia B, Gu M. A metamaterial emitter for highly efficient radiative cooling. Adv Opt Mater 2015;3(8):1047–51.
[27] Zou C, Ren G, Hossain MM, Nirantar S, Withayachumnankul W, Ahmed T, et al. Metal-loaded dielectric resonator metasurfaces for radiative cooling. Adv Opt Mater 2017;5(20):1700460.
[28] Mandal J, Jia M, Overvig A, Fu Y, Che E, Yu N, Yang Y. Porous polymers with switchable optical transmittance for optical and thermal regulation. Joule 2019;3(12):3088–99.
[29] Hossain MM, Gu M. Radiative cooling: Principles, progress, and potentials. Adv Sci 2016;3(7):1500360.
[30] Shi Y, Li W, Raman A, Fan S. Optimization of multilayer optical films with a memetic algorithm and mixed integer programming. ACS Photonics 2018;5(3):684–91.
[31] P. Garg, "A comparison between memetic algorithm and genetic algorithm for the cryptanalysis of simplified data encryption standard algorithm," 2010. *arXiv e-prints*, p. arXiv:1004.0574.
[32] Kischkat J, Peters S, Gruska B, Semtsiv M, Chashnikova M, Klinkmu¨ller M, Fedosenko O, Machulik S, Aleksandrova A, Monastyrskyi G, Flores Y, Masselink WTed. Mid-infrared optical properties of thin films of aluminum oxide, titanium dioxide, silicon dioxide, aluminum nitride, and silicon nitride. Appl Opt 2012;51(28):6789–98.
[33] Palik E. Hand book of optical constants of solids. 1st Edition; 1997.
[34] Pin˜ol L, Rebello K, Caruso K, Francomacaro AS, Coles GL. Physical vapor deposition and patterning of calcium fluoride films. J Vac Sci Technol A 2011;29(2):021001.
[35] Zhao B, Hu M, Ao X, Chen N, Xuan Q, Su Y, Pei G. A novel strategy for a building-integrated diurnal photovoltaic and all-day radiative cooling system. Energy 2019;183:892–900.
[36] Ko B, Lee D, Badloe T, Rho J. Metamaterial-based radiative cooling: towards energy-free all-day cooling. Energies 2019;12(1).
[37] "Mauna kea sky transmission, gemini observatory," 1992.
[38] Huang X, Li N, Wang J, Liu D, Xu J, Zhang Z, Zhong M. Single nanoporous mghpo4•1.2h2o for daytime radiative cooling. ACS Appl Mater Interfaces 2020;12(2):2252–8 PMID: 31886998.
[39] Li Y, Li L, Guo L, An B. Systematical analysis of ideal absorptivity for passive radiative cooling. Opt Mater Express Aug 2020;10:1767–77.
[40] Kecebas MA, Menguc MP, Kosar A, Sendur K. Spectrally selective filter design for passive radiative cooling. J Opt Soc Am B Apr 2020;37:1173–82.
[41] Aguilar-Rivera R, Valenzuela-Rendón M, Rodríguez-Ortiz J. Genetic algorithms and darwinian approaches in financial applications: a survey. Expert Syst Appl 2015;42(21):7684–97.